ADVANCED FUNCTIONAL MATERIALS
www.afm-journal.de

Photophysics of Two-Dimensional Perovskites—Learning from Metal Halide Substitution

*Simon Kahmann, Herman Duim, Hong-Hua Fang, Mateusz Dyksik, Sampson Adjokatse, Martha Rivera Medina, Matteo Pitaro, Paulina Plochocka, and Maria A. Loi**

2D perovskites offers a rich playing field to explore exciton physics and they possess a great potential for a variety of opto-electronic applications. Whilst their photophysics shows intricate interactions of excitons with the lattice, most reports have so far relied on single compound studies. With the exception of variations of the organic spacer cations, the effect of constituent substitution on the photophysics and the nature of emitting species, in particular, have remained largely under-explored. Here PEA_2PbBr_4, PEA_2PbI_4, and PEA_2SnI_4 (where PEA stands for phenylethylammonoium) are studied through a variety of optical spectroscopy techniques to reveal a complex set of excitonic transitions at low temperature. Weak high-energy features are attributed to vibronic transitions breaking Kasha's, for which the responsible phonons cannot be accessed through simple Raman spectroscopy. Bright peaks at lower energy are due to two distinct electronic states, of which the upper is a convolution of the free exciton and a localized dark state and the lower is attributed to recombination involving shallow defects. This study offers deeper insights into the photophysics of 2D perovskites through compositional substitution and highlights critical limits to the communities' current understanding of processes in these compounds.

1. Introduction

What is the impact of metal and halide substitution in two-dimensional perovskites? How does it affect the optical properties of these layered compounds and can we attain deeper insights into the materials' photophysics through comparison? 2D perovskites consist of metal halide (BX_6) octahedra sandwiched between long organic spacer molecules (A) that impose the low-dimensional electronic character through both a quantum and a dielectric confinement of charge carriers into the inorganic layer. As a result of this confinement, the exciton binding energy in these systems exceeds 100 meV[1] leading to a bright luminescence that renders 2D perovskites hot contenders for opto-electronic applications, light-emitting devices in particular.[2] This also demands for a thorough understanding of these compounds' photophysics, as formulated in the preceding questions.

Reflecting the focus of 3D metal halide perovskite research (HaPs), most studied compositions in the 2D field have so far been based on Pb as the B-site metal cation. Most commonly, either iodide or bromide have been used as halide anion on the X-site, to obtain, for example, green or blue luminescence.[3] As suggested by these different colors, halide variation strongly impacts the materials' band gap.[4] A larger variety of organic moieties has been employed as the A-site spacer cation, of which the prototypical molecules are butylammonium (BA^+) or phenylethylammonium (PEA^+). The effect of the A-site cation on the optical properties is generally smaller; besides the straightforward change of the confinement through variations in layer separation and permittivity, the molecules also

S. Kahmann, H. Duim, H.-H. Fang, S. Adjokatse, M. Rivera Medina, M. Pitaro, M. A. Loi
Photophysics and OptoElectronics
Zernike Institute for Advanced Materials
University of Groningen
Nijenborgh 4, Groningen, AG 9747, The Netherlands
E-mail: m.a.loi@rugl.nl

The ORCID identification number(s) for the author(s) of this article can be found under https://doi.org/10.1002/adfm.202103778.

DOI: 10.1002/adfm.202103778

S. Kahmann
Cavendish Laboratory
University of Cambridge
JJ Thomson Avenue CB30HE, Cambridge, UK

H.-H. Fang
State Key Laboratory of Precision Measurement Technology and Instrument
Department of Precision Instrument
Tsinghua University
Beijing 100084, China

M. Dyksik, P. Plochocka
Laboratoire National des Champs Magnétiques Intenses
UPR 3228, CNRS-UGA-UPS-INSA, Toulouse 31400, France

M. Dyksik, P. Plochocka
Department of Experimental Physics
Faculty of Fundamental Problems of Technology
Wroclaw University of Science and Technology
Wroclaw 50-370, Poland

impact the position and the degree of distortion of the inorganic species.[4–7]

Given the large binding energy, these compounds are excellent systems for studying exciton physics. Low temperature studies offer complex data on both absorption and light emission characteristics, which are hotly debated in the field. Especially phenylethylammonium lead iodide (PEA_2PbI_4) has recently become a working horse with reports claiming biexciton emission,[8] large exchange interaction splitting,[9] defect-induced luminescence,[10] pronounced hot exciton luminescence,[11] and the formation of exciton polarons.[12] The nature and the impact of carrier-phonon interactions, as considered in the latter reports, are also of general importance to the wider field of HaP research. Many unusual phenomena, such as long carrier lifetimes, broad Raman spectra, or broad luminescence bands have been linked to phonons and their interaction with charge carriers.

As mentioned above, with few exceptions including different spacer cations or tin incorporation,[13–16] photophysical studies have so far relied predominantly on lead iodide-based compounds with either BA or PEA as the A-site cation. Studied phenomena have thus typically been considered irrespective of related compounds in the broader field of the compositional space. In other words, the impact of the metal and halide constituents has so far remained critically under-explored.

Here we aim to fill this gap of knowledge and we provide an in-depth study of the photophysical properties of a set of 2D HaPs based on PEA as the A-site cation. Additional to the standard PEA_2PbI_4 compound, we introduce bromide as alternative halide on the X-site and tin as substituent of lead on the B-site. We focus our study on the nature of the excitonic properties around the band edge and consider our results in the framework of current discussions in the field. We find that all compounds give rise to an intricate sub-structure of PL peaks at low temperature and we focus our analysis on three main aspects: i) high energy luminescence directly mirrors absorption features and is consequently linked to the recombination of hot excitons that violate Kasha's rule. Our variational approach allows us to show that a simple one-to-one correspondence between A-site vibrational modes detected in Raman spectroscopy, and the spacing of this vibronic progression is invalid. ii) Bright luminescence at lower energy is attributed to diffusion limited recombination involving defects. iii) The main emission peak is a convolution of the free exciton and a localized dark state, as shown through magneto-PL studies.

2. Results

We prepared a set of compounds based on phenylethylammonium (PEA) as the A-site spacer cation. Additional to the prototypical lead iodide-based compound, we considered the variants based on lead bromide and tin iodide. The layered structure of the films, highlighted in **Figure 1**a, forms in out-of plane direction, meaning that the organic and inorganic slabs run parallel to the sample surface, as confirmed by X-ray diffraction (Note S1, Supporting Information). As expected, the compounds possess distinctly different appearances both under white light and in particular under UV illumination, as shown in Figure 1b. Analogous to their 3D counterparts, the valence

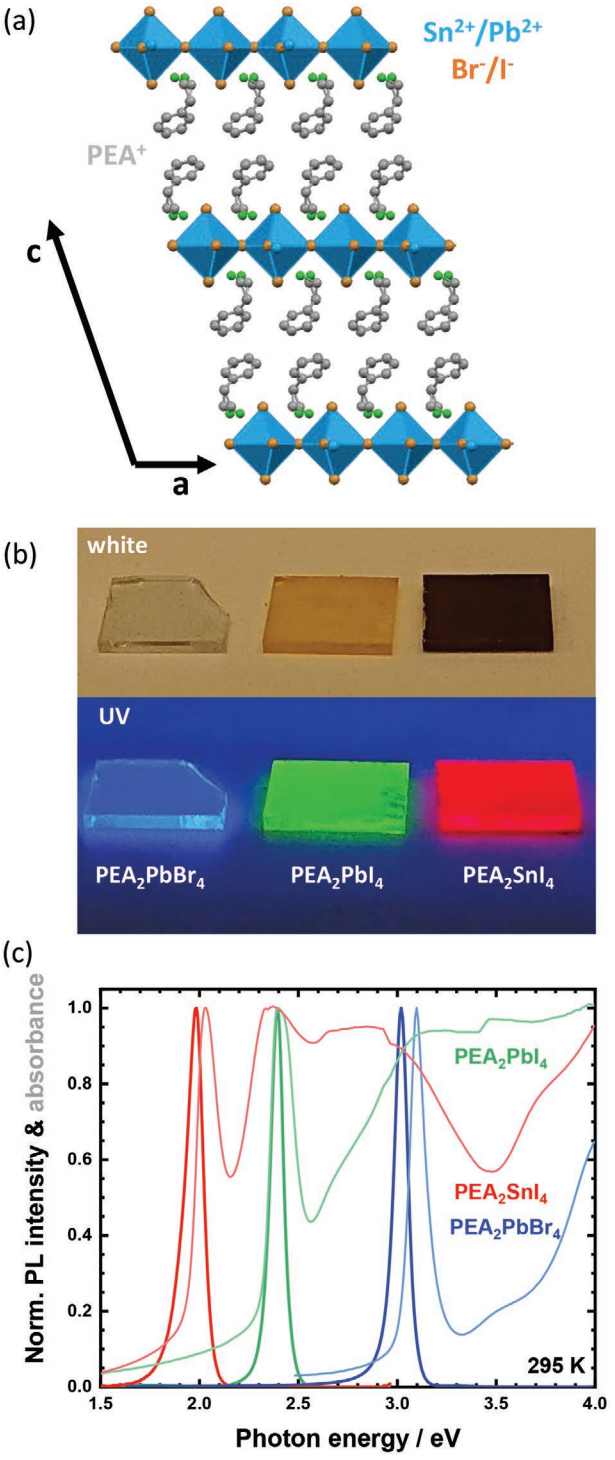

Figure 1. a) PEA_2BX_4 crystal structure incorporating alternating layers of metal halide cages and PEA^+ spacer cations. b) Photographs taken under white light (top) and UV-illumination (bottom). c) Absorbance (lighter colors) and PL spectra (darker) at room temperature exhibit a strong excitonic resonance with a small Stokes shift. Spectra are normalized to the exciton transition. $\lambda_{ex} = 4.6$ eV for PEA_2PbBr_4, else 3.1 eV.

band maximum of 2D perovskites is determined by the metal's outermost s-orbital and the halide's p-orbital, whilst the conduction band is determined by a combination of the metal and

halide p-orbitals as well as the metal p and halide s-orbital.[17,18] Variation of the constituent metal and halide species thus widens the gap for smaller halides and narrows it when substituting lead with tin.[19] This translates into the shifted absorption onset and PL peak energy shown in Figure 1c.

Smaller contributions to the band gap energy arise from different degrees of distortion in the inorganic layer. As we discuss in Note S1, Supporting Information, the here employed compounds exhibit largely similar degrees of distortion. This is highly beneficial, as it allows for drawing conclusions based on the chemical nature of the substituted constituents without the need to assess secondary impacts from changes in the crystal structure.

All studied compounds exhibit a narrow absorption band due to the exciton and strongly increasing absorption of continuum transitions toward high energy. The luminescence is governed by a narrow emission and a small Stokes shift, whose shape and position are independent of the incident laser power (Figure S1, Supporting Information). The PL intensity furthermore scales linearly with the incident power, which all underlines the excitonic origin of the luminescence.

Before focusing on the main issues of this report, we would like to note that in a stark contrast to the 3D compounds,[20,21] the time resolved PL of the lead-iodide compound decays significantly faster than that of the tin-based variant. The latter gives rise to a persistent PL tail ranging toward the microsecond time scale (Figure S2, Supporting Information), indicating the formation of long-lived states upon photoexcitation.

At low temperature, the narrow band edge emission splits into a rich substructure, as shown in **Figure 2**. The intensity of these lines varies over several orders of magnitude and each spectrum is centered around two pronounced emission lines, X_1 and X_2 with one or two weak peaks at higher energy and broader contributions at energies below. **Table 1** summarizes the positions.

To understand the origin of the PL, it is expedient to consider the luminescence in context of the samples' absorption. Figure 2 displays the corresponding data in panels (a–c). In contrast to the room temperature spectra in Figure 1c, also the absorbance develops a distinct substructure upon cooling. Instead of a mere narrowing of the 1s exciton line, several absorption peaks emerge on the high energy side (note that PEA_2PbI_4 is partially saturated around 2.35 eV). The X_1 emission exhibits a small Stokes shift relative to the lowest absorption peak for all three cases and we thus conclude that X_1 is due to the recombination of the ground state (GS) exciton.

Moreover, all three samples give rise to at least one distinct absorption peak on the high energy side that coincides with either X′ or X″ and a close look reveals that all observable PL lines at high energy coincide with distinct absorbance features (also consider Figure S4, Supporting Information). Importantly, the small Stokes shift and the overlap of PL and absorbance can lead to significant reabsorption of the luminescence affecting magnitude and shape of the observed features.

Given their similarities around the band edge, we replotted the PL spectra in Figure 2d. The high energy peaks of all three samples lie within a range of 150 meV from the main emission peak X_1. For PEA_2PbI_4 and PEA_2SnI_4, the X′ and X″ are virtually equidistant lying at 45 and 87 meV and 60 and 113 meV for Pb and Sn, respectively (consider Table 1). Both peaks of the latter compound are furthermore much broader than for the lead-based samples and clearly asymmetric. Further weak contributions can be identified in the background. PEA_2SnI_4, for example, exhibits a small PL signal around 25 meV, which underlines the complexity of the observed spectra and how spectral broadening likely obscures the true number of transitions. We focus on the most pronounced signals that can be clearly identified. PEA_2PbBr_4 only exhibits one distinct PL peak

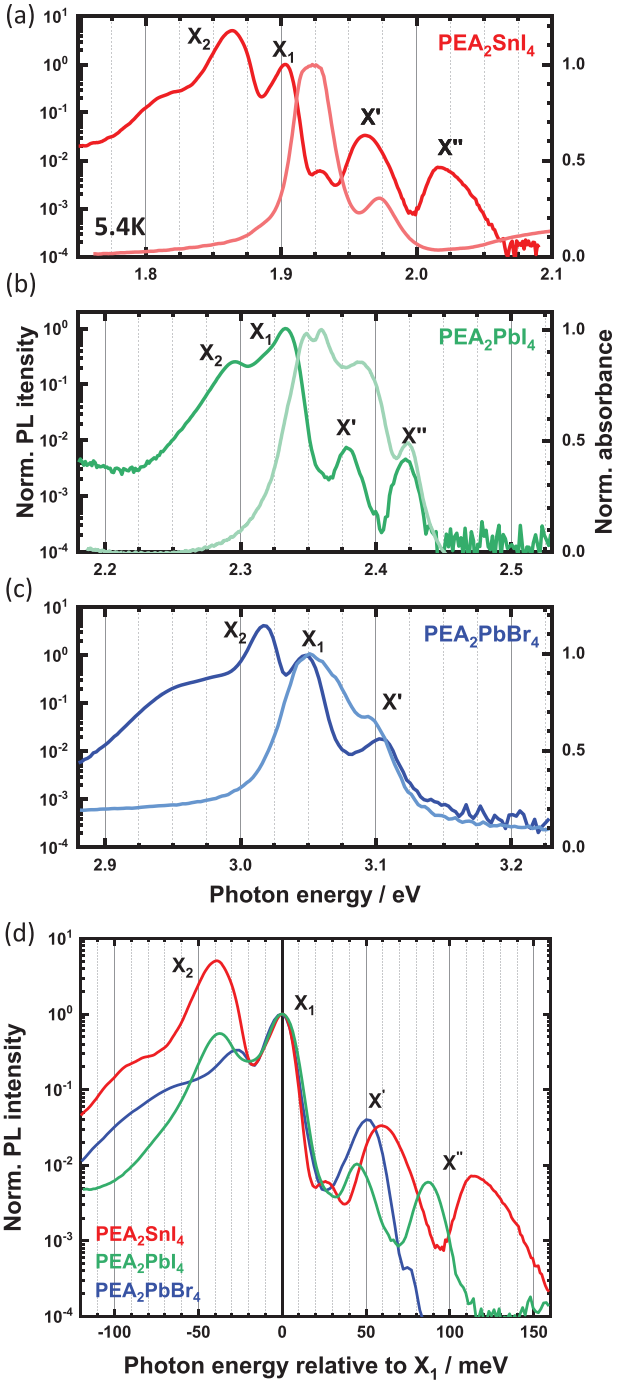

Figure 2. a–c) PL spectra of the three compounds at 5.4 K normalized to the upper main peak, X_1 with corresponding normalized absorbance spectra. Note the logarithmic intensity axis of the luminescence. d) PL spectra aligned with respect to X_1.

Table 1. PL peak position at 5.2 K given in eV and their distance from X_1 in meV in parentheses.

Compound	X_2	X_1	X′	X″
PEA_2PbBr_4	3.012 (−31)	3.043 (–)	3.095 (51)	–
PEA_2PbI_4	2.298 (−38)	2.334 (–)	2.379 (45)	2.422 (87)
PEA_2SnI_4	1.863 (−39)	1.903 (–)	1.962 (60)	2.017 (113)

X′ above X_1 (≈51 meV), which we assume is due to the diminishing detector sensitivity at even higher energy ($E > 3.2$ eV).

The symmetry between the absorption and the high energy luminescence shows that the respective peaks originate from the same transitions. Considering the similar spacing of the high energy features, the structure can be understood as a Frank–Condon series. The observed absorption peaks link the electronic ground state to a progression of vibrational levels of the excited state (ES), as depicted in **Figure 3**a. The corresponding PL lines analogously stem from the inverse process. In other words, X′ and X″ recombination occurs from excited vibrational sub-levels, so-called hot excitons, which is in express violation of Kasha's rule. The separation of X′ and X″ thus results from the coupling of excitons to vibrational modes of energy E_{vib}.

We note that one might consider these features to be due to a Rydberg series, but both their spacing as well as their common shift in magnetic fields rule out this possibility, as recently reported for the iodide-based compounds.[7,22]

Such a vibronic progression was proposed for PEA_2PbI_4 before[11] and the dominant mode coupling to the exciton was said to stem from the spacer molecule on the A-site; a claim subsequently backed up by considering several A_2PbI_4 compounds.[14] In this light the large differences in spacing between the current samples surprise, seeing that the compounds are all based on PEA on the A-site. Certainly, the interplay of the molecules with different inorganic species will affect the energy of relevant vibrational modes, but the small differences in crystal structure and distortion (Note S1, Supporting Information), render a 15 meV difference between PEA_2SnI_4 and PEA_2PbI_4 unexpectedly large.

We therefore monitor the vibrational structure of the compounds through non-resonant Raman scattering (λ = 785 nm; 1.58 eV; for further discussion consider Note S2, Supporting Information). Pronounced Raman signals in HaPs typically stem from the inorganic components found in the region below 80 cm^{-1} (10 meV).[23] These features are evident in Figure 3b, which compares the low energy region at room temperature and at 4.3 K. Temperature reduction allows for distinguishing a rich subset of peaks that appears as broad features at elevated temperature. The strong response obtained from PEA_2PbI_4 and PEA_2SnI_4 facilitates the direct comparison to extract the impact of metal variation on the energy of vibrational modes. The shift of dominant peaks in the low energy region is small (≈1 meV). In contrast, a stronger shift (and smaller response) manifests for PEA_2PbBr_4, which is in accordance with previous data.[24]

The spectral region directly corresponding to the separation of the hot luminescence is shown in Figure 3c. The scattering

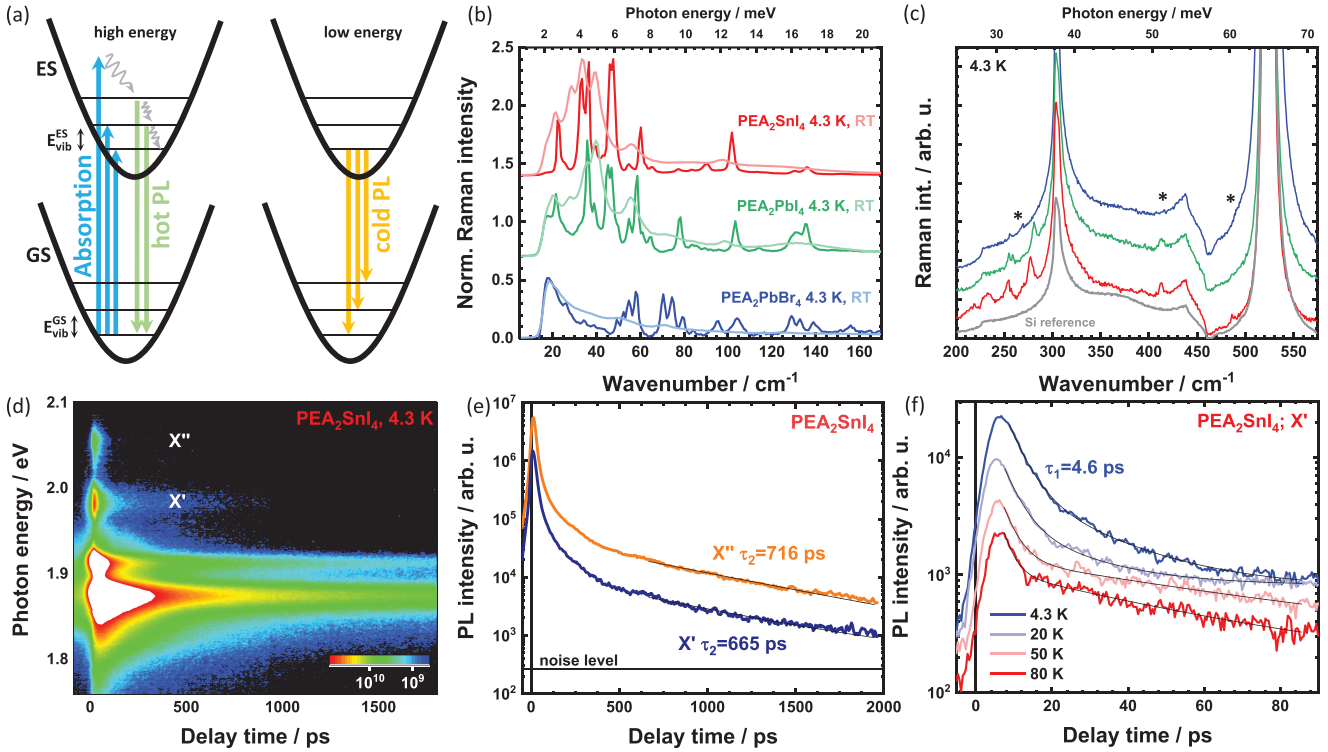

Figure 3. a) Relevant transitions of the absorbance, hot, and cold luminescence sketched in a Frank–Condon framework. b) Non-resonant Raman spectra at room temperature and at 4.3 K in the low energy region. c) Region corresponding to the spacing of the high energy PL lines, as indicated by asterisks. The pronounced background stems from the silicon substrate shown in gray. d) Streak camera plot of the PEA_2SnI_4 PL at 4.3 K and e) corresponding extracted decay curves of the hot luminescence. f) Short delay decay dynamics upon temperature variation.

intensity of modes in this region is several orders of magnitude smaller and the spectra are dominated by well known features from the silicon substrates.[25] Nonetheless, several signals from the perovskites can be identified and the respective regions of interest are indicated. Phonon modes at this energy can in part be attributed to the organic moiety.[11,22,26] Given its comparable energy, the phonon pair around 32 meV was previously said to determine the spacing of PEA_2PbI_4 by coupling to the excitons.[22] Considering the current results, such a direct correspondence should be made with care: not only is this energy significantly smaller than the PL spacing of 45 meV, but these Raman modes appear similarly also for PEA_2SnI_4 and for PEA_2PbBr_4, whose PL peaks are separated by ≈60 and 50 meV. Conversely, a minor feature around 60 meV in the Raman spectrum of PEA_2SnI_4, which one might identify as the coupling mode, can also be observed for PEA_2PbI_4.

Obviously, there is a discrepancy between the differences in the spacing of PL/absorption peaks and the uniformity of the Raman spectra in the relevant spectral region. There is no direct correspondence between the observable Raman modes and the separation of features in PL/absorption. This means that despite clear evidence from magneto-absorption[7] and spectral symmetry for a vibronic progression to determine the high energy PL and absorption lines, the mechanism of exciton phonon coupling remains elusive. Straightforward attempts linking the energy of Raman modes to the spacing are inadequate and the lack of direct correspondence requires further investigations. A possible explanation might be strong differences between the vibrational properties of the ground state (E_{vib}^{GS} probed in Raman spectroscopy and the excited state (E_{vib}^{ES}), which determines the spacing in hot PL and absorbance (Figure 3a). So far reported data on the ES have shown great similarities with the GS,[26] but the current data clearly warrant further study.

Hot exciton recombination competes with the relaxation toward the lowest excited state, as sketched in Figure 3a. Additional to a low intensity of X′ and X″, this should result in a short lifetime of the hot luminescence. Not surprisingly, reported lifetimes for X′ and X″ lie well below 10 ps.[11,14] In stark contrast, Figure 3d shows a streak camera image (PEA_2SnI_4; 4.3 K) that displays a long-lived tail for X′. The decay curves prove this to be true for both hot peaks (Figure 3e). The initial rapid decay (resolution limited around $\tau_1 = 4.5$ ps) reduces the signal by two orders of magnitude, but is followed by a second, much slower process with a lifetime of around 700 ps. The presence of this two-stage decay is similarly observed at elevated temperature, where the fast initial decay becomes less dominant (Figure 3c), and it is analogously present for the two lead-based compounds (Figure S5, Supporting Information).

To the best of our knowledge, this long-lived process has so far not been observed. Based on its presence in all three compounds, we infer that it is a general characteristic of 2D HaPs. The slow decay of X′ and X″ luminescence seems to conflict with the rapid relaxation of excitons toward the lowest vibrational level of the ES. As possible explanations, Auger processes or exciton–exciton annihilation could promote relaxed excitons into higher states and thereby repopulate excited vibrational levels. In this case, we would expect a strong dependence of the PL lifetime on the excitation intensity, but we found τ_2 to remain unaffected over the excitation range accessible to us. An alternative explanation could be the retarded recombination of free charge carriers. Given that the employed high energy excitation initially generates free charge carriers, it is possible for a small, but finite, population of charge carriers to remain unbound and to only form excitons at a later stage. The long-lived PL tail of X′ and X″ would thus be dictated by the lifetime of free charge carriers and not by the exciton relaxation. Notably, some evidence for such persistent charge carriers was reported recently.[27]

In the following, we turn to the low energy side of the spectra, to what can be termed the cold luminescence from relaxed states. As evident from Figure 2, all three samples exhibit a second pronounced PL peak (X_2) and further smaller contributions below X_1 at low temperature. We focus on signals shifted by less than ≈50 meV, noting that features at lower energy involve either shallow or deep defects.[10]

Based on the above discussion and on low temperature spectra alone, one might assume the structure of low energy luminescence to be merely due to transitions toward higher vibrational levels of the GS, as shown in Figure 3a on the right. As we elaborate in the following, the analysis of temperature dependent and time resolved PL shows that this is not the case.

We discuss the temperature dependent changes in more detail in Note S3, Supporting Information (absorbance, steady state, and transient PL; Figures S10–S14, Supporting Information) and focus here on the following aspect: the emergence of additional peaks does not merely follow from a narrowing of spectral features, but by drastic changes in PL intensity and intensity ratios, as shown in **Figure 4**a–f. For PEA_2SnI_4 the trend is relatively straightforward: below 140 K the emission splits into two strong peaks, X_1 and X_2 (Figure 4a), of which X_2 becomes increasingly more pronounced upon cooling (Figure 4d; Figure S12, Supporting Information).

The lead-based compounds show more complex behaviors. PEA_2PbI_4 also exhibits a splitting of PL peaks, but whereas X_2 and a third state between X_1 and X_2 (termed * and discussed below) are dominant from 70 K on, X_1 is again the strongest below 20 K. Similarly, the bromide-based variant exhibits a complex trend of several weaker sub-peaks around 3 eV over the intermediate temperature region, but it is only around 20 K and below, where X_2 becomes dominant.

The transient PL shows strikingly different dynamics for the two main peaks at low temperature (shown in Figure 4g–i). X_1 exhibits a fast initial intensity reduction that is accompanied by a red-shift–particularly pronounced for PEA_2SnI_4 and PEA_2PbI_4. X_2, on the other hand, shows a less pronounced spectral shift, but a clear delayed onset of the intensity. The extracted transients are discussed in Note S4, Supporting Information (Figures S15– S17, Supporting Information), where we also employ two-photon excitation to show the red-shift to not be an artefact from reabsorption. Note that despite our focus on the early stage of the decay, the overall luminescence lifetime lies in the range of microseconds (Figures S2 and S3, Supporting Information).

The interplay of the two states can best be illustrated when considering the relatively simple case of PEA_2SnI_4. **Figure 5**a,b shows the temperature dependent dynamics of X_1 and X_2 at short delay time. Cooling increases the prompt PL intensity in both cases, probably due to the suppression of phonon-assisted

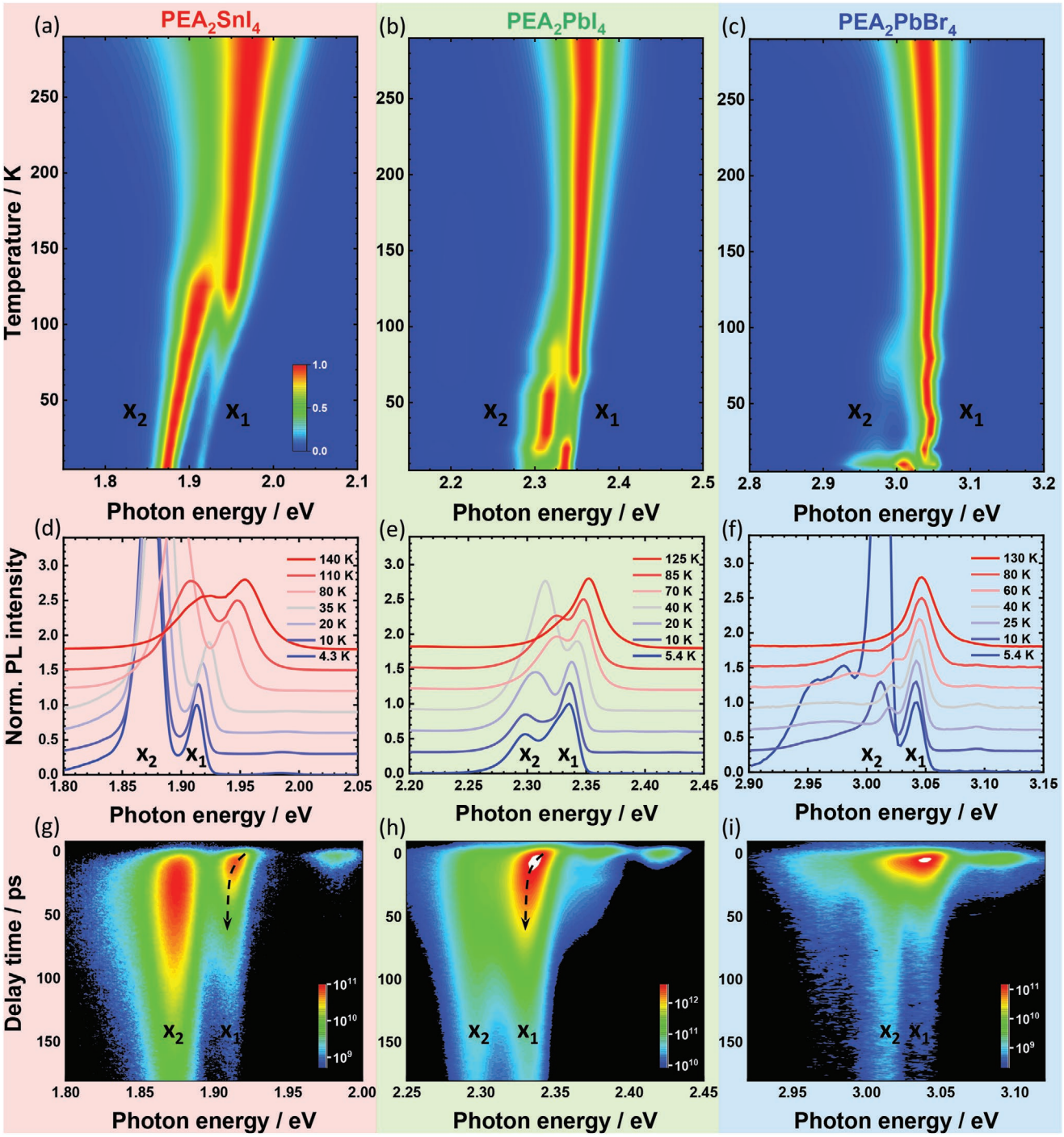

Figure 4. Temperature dependent PL of the three materials normalized to a global maximum in (a–c) and to X_1 in (d–f). Spectra in (d–f) are vertically offset. Temperature variation has a profound effect on the luminescence in each case and the trends cannot be explained through a vibronic progression. Early time transient PL at minimum temperature in (g–i) highlights a delayed maximum for X_2 and a time-dependent red-shift of X_1 at early delay, indicated by the dashed arrow.

non-radiative decay channels. However, whereas X_2 retains this higher intensity over time, X_1 shows an increasingly pronounced rapid initial decay component with τ = 12–15 ps. At 170 K the decay is almost monoexponential, but becomes clearly biexponential below. This trend is similarly observable when considering longer delays up to 2 ns, as shown in Figure S12, Supporting Information. Simultaneously, X_2 exhibits a monoexponential decay at 170 K with an increasingly pronounced delayed maximum upon cooling (black arrow in Figure 5b).

The pronounced spectral changes upon temperature variation along with the stark differences in early decay dynamics exclude a vibronic progression as the dominant mechanism

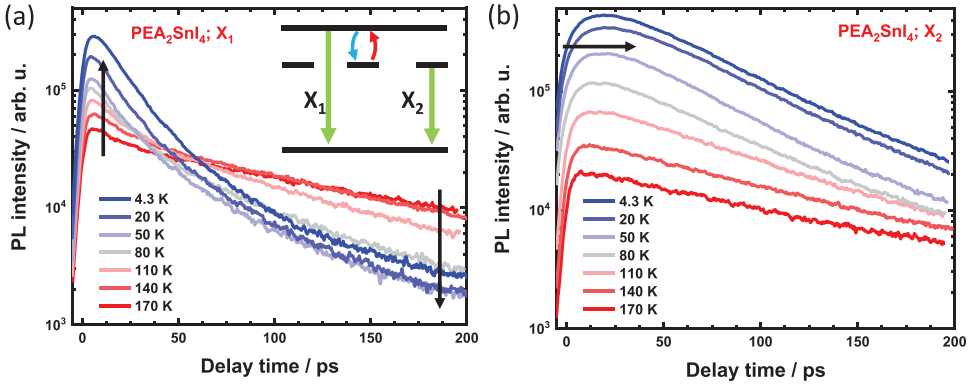

Figure 5. Temperature dependent PL for a) X_1 and b) X_2 of PEA_2SnI_4 at short delays. Cooling increases the overall initial intensity for both peaks, but a fast decay component becomes increasingly dominant for X_1 at low temperature and a delayed maximum forms for X_2. The interplay is explained through a two-state model with a diffusion step, as shown in the inset of (a).

behind X_1 and X_2. These transitions would otherwise follow identical dynamics, as they would originate from the same state (Figure 3a) and their relative intensity should be independent of the temperature. Moreover, as shown in Figure S6, Supporting Information, PbI_2 exhibits a similar behavior, which rules out a mechanism involving the organic moiety.

Historically, the X_2 luminescence in these layered systems has often been attributed to the recombination of biexcitons to form the so-called M-band.[8,28–30] This was commonly based on a superlinear dependence of the PL intensity on the excitation fluence. Although biexcitonic emission seems already to be excluded from the dynamics discussed above, we nonetheless consider the impact of varying the excitation intensity to clarify this point. As we discuss in Note S5, Supporting Information (Figures S18–S20, Supporting Information), the power dependent measurements on our films reveal two important insights: First, the intensity of X_1 scales linearly with the fluence and correlates with the intensity of X′ and X″. This underlines their shared origin, as discussed in the first part of this manuscript. Second, there is no uniform dependence of X_2 on the excitation power: PEA_2SnI_4 is strongly superlinear, PEA_2PbBr_4 sublinear, and PEA_2PbI_4 becomes superlinear at high power. The spectra are additionally subject to irreversible changes upon high intensity exposure. PEA_2SnI_4, in particular, exhibits a much more pronounced X_2 emission after high intensity exposure, rendering the superlinearity an artefact of irreversible sample changes. In accordance with data on single crystals,[16] we conclude that biexcitons play no role in the observed emission.

In contrast, when considering X_2 relative to the absorption, as in Figure 2, one finds that the emission coincides with a tail below the first absorption maximum in all three cases. Above discussed data plotted on a logarithmic axis (Figure S4, Supporting Information) show that for some cases this tail exhibits a clearly resolvable absorption peak, which is in accordance with previous reports.[9,26,31,32] There is thus a second distinct and optically allowed electronic state below the 1s exciton.

Combined with the delayed onset dynamics and the temperature dependence of the luminescence intensity, we propose the model sketched in the inset of Figure 5a. X_1 and X_2 are due to two distinct electronic transitions, the free exciton, in case of X_1, and a transition involving shallow defects, in case of X_2. Thermal repopulation of X_1 from X_2 (with an activation energy of 36.7 meV in case of PEA_2SnI_4 (Figure S12, Supporting Information), occurs at elevated temperature, but is suppressed upon cooling. This generates the rapid initial decay of X_1. At the same time, the slowed down transfer toward X_2, as indicated by the increasingly delayed onset toward low temperature, can be interpreted as X_2 emission to be preceded by diffusion toward the defect.

We note that more recently, PL peaks below X_1 have become a hot topic with explanations invoking a variety of mechanisms including defects at grain boundaries,[33] a magnetic dipole transition,[34,35] and the formation of distinct excitons due to interaction with phonons.[36,37] Several reports refer to the strong dependence of the detection direction and polarization conditions relative to the lattice planes, with the lower transition particularly prominent for in-plane detection.[33,34,36] In principle, our data are congruent with the proposition of defects at grain boundaries, as put forward by Wang et al.,[33] but since X_2 is similarly observed for single crystals, grain boundaries alone appear to be an unlikely origin. In our view, propositions that invoke polaronic effects, such as self-trapping, also fail to explain the corresponding absorption, the strong non-linear and partly irreversible effect of laser power, as well as the delayed maximum in the transient PL.

Taken together, the above evidence makes shallow defects and bound excitons strong contenders for the origin of X_2: although detectable, its absorption is much lower than the 1s transition associated with X_1. Furthermore, it coincidences energetically with shallow defects in PbI_2 (Figure S6, Supporting Information) as well as bound excitons in bulk perovskites,[38] and exhibits an activation energy similar to one attributed to shallow traps in diffusion experiments on PEA_2PbI_4 single crystals.[39] Non-linearities and irreversible changes of the PL intensity could easily be explained through the well-known photoactivation of halide-related defects.[40–43]

One of the remaining phenomena to account for is the prominent red-shift of X_1 at short delays and lowest temperatures (Figure 4g,h) observed specifically for the iodide-based variants (highlighted also in Figures S15– S17, Supporting Information). Given the small Stokes shift of X_1, one might think the spectral shift to be due to increased reabsorption upon carrier diffusion into the bulk of the film, but as magneto-PL studies further underline, X_1 at this temperature is actually the convolution of at least two states, the free exciton and a localized state.

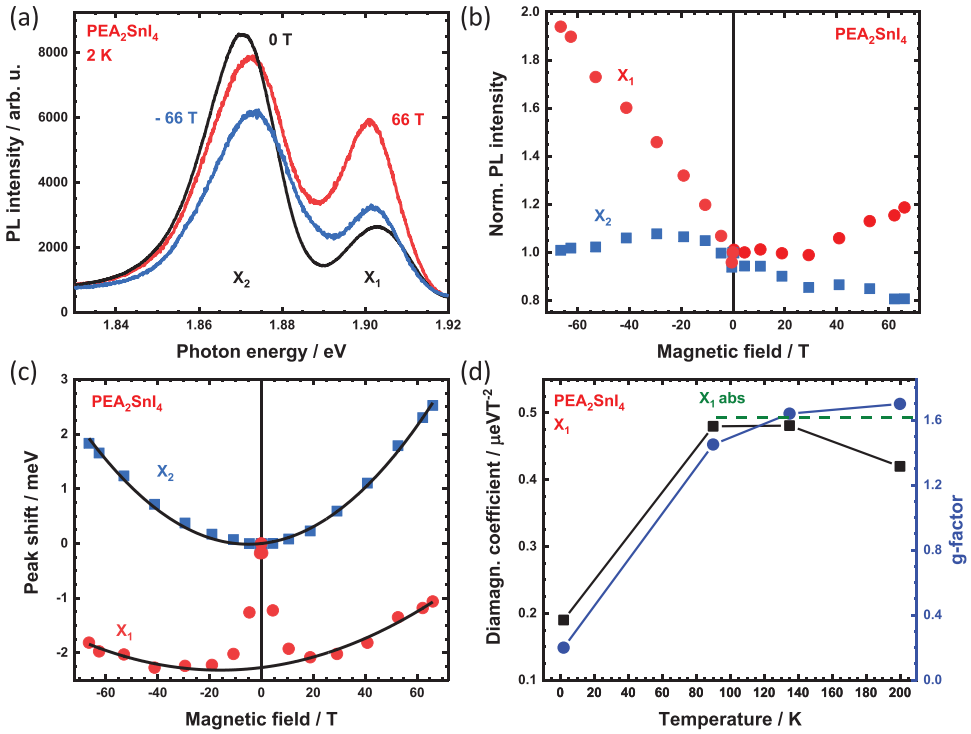

Figure 6. Magneto-photoluminescence data of PEA_2SnI_4 at 2 K. a) Absolute PL spectra under 66 T field of opposite polarities (red and blue lines) and in zero field condition. b) Integrated PL intensity of X_1 and X_2 relative to zero field condition as a function of the magnetic field. c) Extracted peak position; black lines indicate fits to Equation (1). d) Temperature dependence of the diamagnetic coefficient (black) and *g*-factor (blue) of X_1. The dashed red line indicates the *g*-factor of the 1 s exciton absorption at 2 K.

Figure 6a shows the PL of PEA_2SnI_4 when applying a magnetic field of 66 T in out-of-plane direction (Faraday configuration) at 2 K along with the spectrum under zero field condition. We probed the emission of σ^+ and σ^- circularly polarized light (red, blue) and find the intensity of X_1 to increase for both field directions (Figure 6a,b), whereas X_2 decreases slightly under high field strengths. Additional to the changes in intensity, the two main peaks also undergo a field-dependent energy shift, illustrated in Figure 6c. The black lines indicate fits to the interplay of Zeeman splitting and diamagnetic shift, as discussed below, but the low-field behavior of X_1 shows an uncharacteristic red-shift of ≈2 meV.

Whereas brightening is generally attributed to either an increased oscillator strength imposed by a B-field induced reduction of the exciton's spatial extent or by the intermixing of bright and dark states, [44–47] the low-field red-shift of X_1 clearly points to the presence of a lower lying state that brightens at higher field strengths. Such a field-induced brightening of the lower lying state is more clearly observed in the case of PEA_2PbI_4 (Note S6, Supporting Information.)

Additional insight can be obtained when considering how the diamagnetic shift and the Zeeman effect impact the luminescence. The magnitude of the exciton energy shift in the low-field limit is given by:[7]

$$\Delta E_{\pm} = \pm 1/2 g_{\text{eff}} \mu_B B + c_0 B^2 \quad (1)$$

in which g_{eff} denotes the effective Landé *g*-factor, μ_B the Bohr magneton and c_0 the diamagnetic coefficient. Fitting Equation (1) to the data in Figure 6c, we find a diamagnetic shift of 0.19 and a *g*-factor of 0.20 for X_1, when excluding the low-field shift (for X_2 the values are 0.51 μeVT^{-2} and 0.17). The diamagnetic shift as well as the *g*-factor are considerably lower than the reported values for the free exciton absorption in this material: $c_0 = 0.68$ μeVT^{-2} and $g_{\text{eff}} = 1.6$.[7] This indicates that low temperature emission occurs from considerably more localized states than the absorbance. When the temperature is raised, c_0 and g_{eff} of the emission increase (Figure 6d) to approach the values corresponding to the free exciton absorption at 2 K (indicated by the dashed red line for g_{eff}).

The picture that emerges for PEA_2SnI_4 is thus as follows: in accordance with the time resolved data, the X_1 emission stems from two states at low temperature, of which the lower one is localized, likely a bound exciton, and becomes increasingly bright under the influence of an external magnetic field. Temperature increase lifts the localization and the overall emission becomes governed by the same transition responsible for photoabsorption, that is the free 1s exciton.

The PEA_2PbI_4 data are largely analogous to the tin-based variant and we discuss the results in Note S6, Supporting Information (Figures S21 and S22, Supporting Information). Notably, what appears as the lower-lying state of X_1 for PEA_2PbI_4 at low temperature (termed *) can be tracked over a wide temperature range as a distinct peak separated from X_1, whereas for the Sn-variant this is not the case.

Splitting of X_1 was recently also reported for single crystals of PEA_2PbI_4 based on a similar experimental approach.[9] In that work, the two peaks were said to be due to two distinct bright states. Alternatively, theoretical considerations and transient PL

studies have led to the proposition of a pair of low-lying dark and higher-lying bright state to form X_1 in PEA_2PbI_4.[8] This line of reasoning followed earlier studies on bromide-based compounds[29] and was also invoked to explain aspects of the temperature dependent PL of PEA_2SnI_4.[15] Importantly, though, these reports base their explanations on properties of the free exciton and do not consider additional extrinsic effects, as suggested by the localization. Splitting into a low-lying dark state and a higher bright state is also a compelling explanation for the long PL lifetime of X_1.

Notably, also a recent report on PEA_2PbI_4 ascribed this dark nature to the localized state at 2.32 eV (what we term *).[45] However, as the original dark-bright splitting was said to be due to the electron–hole exchange interaction of the free exciton,[8,29] the underlying mechanism for this attribution is unclear. Either way, our magneto-PL data show that a mechanism invoked to explain the behavior of X_1 in PEA_2PbI_4 will also have to apply to PEA_2SnI_4.

3. Conclusion

In summary, we studied the photophysics of 2D metal halide perovskites with varied composition of the inorganic constituents. The recombination of free excitons generates a single pronounced emission line at room temperature, which narrows upon sample cooling to reveal an intricate substructure. We attribute high energy features to a vibronic progression from transitions that break Kasha's rule.

Our study highlights a lack in the current understanding of the vibronic progression, as the spacing of the high energy PL lines cannot be traced back to phonon modes observable in Raman spectroscopy and cannot be linked directly to the organic cation on the A-site. Our findings not only warrant further study on the excited state vibrational properties, but also highlight an unexpectedly long-lived tail of the hot emission, whose origin is as yet unclear.

All samples exhibit two main emission lines, of which the upper one is attributed to the 1s exciton. By means of time resolved luminescence and magneto-PL studies, we show that this bright peak generally attributed to free exciton recombination is split into two transitions, of which the lower is due to a localized state that shows evidence of being optically dark. Based on temperature and time-dependent studies, we propose the second bright emission to be due to shallow defects.

Our work underlines the largely similar photophysics of these 2D compounds and shows how metal-halide substitution affects their photophysics. Close study not only reveals important insights, but uncovers several open questions.

4. Experimental Section

Thin Film Preparation: All chemicals were used without further purification. Solutions and thin films were prepared inside of a nitrogen filled glove box. Quartz and n-type silicon with no native oxide were used as substrates. Quartz substrates were sonically cleaned with a soapy solution, deionized water, acetone, and isopropanol, whereas for Si, only the two latter solvents were used. The surface was subsequently treated through UV–ozone for 20 min and thin films were cast a maximum of 15 min after the final treatment step.

PEA_2PbBr_4 thin films: A 2:1 molar ratio of PEABr (⩾98% - Sigma-Aldrich) to $PbBr_2$ (⩾98% - TCI) salts was dissolved in DMSO (>99.8% Alfa Aesar) to prepare 0.5 M precursor solutions. The solutions were ready after 3 h of constant stirring at room temperature. The PEA_2PbBr_4 thin films were spin-coated on top of 1 cm^2 quartz substrates in a single-step process at 5000 rpm for 60 s. 200 µL of toluene (99.8% or 1.5 × 1.5 cm^2 silicon substrates ACROS–organics), as antisolvent, was dripped at the twentieth second after the beginning of the spinning. Right after the spinning process, the films were transported to a hot plate to be annealed at 80 °C for 10 min.

PEA_2PbI_4 and PEA_2SnI_4 thin films: Similarly to the above-mentioned recipe, a 2:1 molar ratio of PEAI (>98% - TCI) to SnI_2 (99.99% - TCI) or to PbI_2 (99.9% -Sigma Aldrich) salts was dissolved in a solution composed of 4:1 volumetric ratio of DMF (99.8%- Sigma Aldrich) and DMSO (>99.8% Alfa-Aesar) to prepare 0.5 M precursor solutions. Kept under constant stirring, the solutions were ready to be spin-coated in a double-step process to form the PEA_2PbI_4 and PEA_2SnI_4 thin films. The first step was carried out at 2000 rpm for 10 s following the second at 8000 rpm for 30 s. 150 µL of chlorobenzene (99.8% Sigma-Aldrich), as antisolvent, was dripped at the fiftieth second after the beginning of the second spin-coating process. The films were annealed at 100 °C for 10 min on a hotplate.

Two sets of samples were prepared for the PL experiments fabricated with a separation of several months to confirm the reproducibility of our insights. When storing the samples under nitrogen, no spectral changes can be observed even after several weeks.

Photoluminescence Spectroscopy: The samples were mounted into a cryostat (Oxford Optistat CF) and excited at 3.1 eV (400 nm) in case of the iodide based compounds and at 4.6 eV (267 nm) for the bromide and chloride based compounds using the second/third harmonic of a mode-locked Ti:sapphire laser (Mira 900, coherent) that emits at a repetition rate of 76 MHz. Steady-state spectra were recorded with a Hamamatsu EM-CCD camera that was spectrally calibrated. Employed gratings had 30 or 150 lines mm^{-1} for the overview and high resolution spectra. The excitation beam was spatially limited by an iris and focused with a lens of 150 mm focal length. The fluence was adjusted using gray filters and the spectra were taken in reflection with an incident angle of ≈60° with respect to the sample surface. Time-resolved traces were taken with a Hamamatsu streak camera working either in synchroscan or single sweep mode. An optical pulse selector was used to vary the repetition rate of the exciting pulses where necessary. Measurements occurred under helium atmosphere.

With exception of the power dependent studies, the incident laser intensity was set to 3 or 10 µW, which corresponds to a fluence range of ≈3 to 11.5 nJ cm^{-2} per pulse upon 400 nm excitation and 7.5 to 25 nJ cm^{-2} per pulse in case of 267 nm excitation. For this estimation we assumed the beam diameter on the sample to be given by

$$d_{\text{focus}} = 1.27 \times f_{\text{lens}} \lambda M^2 / D \tag{2}$$

using the focal length, laser wavelength, the quality factor (assumed to be 1), and the beam diameter incident on the lens (2 mm). Np beam damage was observed at such low intensity levels.

Raman Spectroscopy: Non-resonant Raman scattering was performed using a confocal Raman microoscope (invia, Renishaw) and by using an integrated 785 nm solid state laser. Scattered light was sent through a 15 cm^{-1} low energy edge filter, dispersed with a 1800 l mm^{-1} grating and detected using a silicon CCD panel.

The samples were mounted with silver paste in a cryostat (Oxford, Hires) and kept under vacuum.

Magneto-PL Spectroscopy: Magnetic field dependent measurements were performed at the National Laboratory for Intense Magnetic Fields (LNCMI) in Toulouse, France. For photoluminescence measurements, light from a continuous wave laser was coupled into an optical fibre and passed through a quarter wave-plate and polarizer before exciting the sample. The PL was collected in reflection geometry through the same fiber. The out-coupled light was then directed onto a monochromator and detected using a liquid nitrogen cooled CCD camera. The sample was placed in a liquid helium cryostat that was in turn positioned in the center of a reinforced resistive coil used to generate the external magnetic field.

Measurements were performed in a pulsed magnetic field with a pulse duration of 500 ms and a maximum field strength of 66 T applied in Faraday configuration. By adjusting the direction of the applied magnetic field, different polarization states (σ^+/σ^-) could be accessed.

Supporting Information

Supporting Information is available from the Wiley Online Library or from the author.

Acknowledgements

Arjen Kamp and Teodor Zaharia are thanked for technical support. The authors thank Dr. Graeme Blake for insightful discussions on the crystallography. S.K. is grateful for a research fellowship (Grant No: 408012143) awarded by the Deutsche Forschungsgemeinschaft (DFG). This work was financed through the Materials for Sustainability (Mat4Sus) programme (739.017.005) of the Netherlands Organisation for Scientific Research (NWO). This work is part of the research program of the Foundation for Fundamental Research on Matter (FOM), which is part of NWO. This is a publication of the FOM–focus Group "Next Generation Organic Photovoltaics" participating in the Dutch Institute for Fundamental Energy Research (DIFFER). The project received funding from National Science Centre Poland within the OPUS program (grant no. 2019/33/B/ST3/01915). This work was partially supported by the OPEP project, which received funding from the ANR-10-LABX-0037-NEXT. M.D. appreciates support from the Polish National Agency for Academic Exchange within the Bekker programme (grant no. PPN/BEK/2019/1/00312/U/00001). The Polish participation in the European Magnetic Field Laboratory is supported by the DIR/WK/2018/07 grant from Ministry of Science and Higher Education, Poland.

Conflict of Interest

The authors declare no conflict of interest.

Data Availability Statement

The data that support the findings of this study are available from the corresponding author upon reasonable request.

Keywords

2D perovskites, defects, excitons, magneto-photoluminescence, photophysics, Ruddlesden-Popper phases

Received: April 21, 2021
Revised: July 19, 2021
Published online: August 11, 2021

[1] T. Ishihara, J. Takahashi, T. Goto, *Solid State Commun.* **1989**, *69*, 933.
[2] L. Zhang, C. Sun, T. He, Y. Jiang, J. Wei, Y. Huang, M. Yuan, *Light Sci. Appl.* **2021**, *10*, 61.
[3] J.-C. Blancon, J. Even, C. C. Stoumpos, M. G. Kanatzidis, A. D. Mohite, *Nat. Nanotechnol.* **2020**, *15*, 969.
[4] E. I. Marchenko, S. A. Fateev, A. A. Petrov, V. V. Korolev, A. Mitrofanov, A. V. Petrov, E. A. Goodilin, A. B. Tarasov, *Chem. Mater.* **2020**, *32*, 7383.
[5] K.-Z. Du, Q. Tu, X. Zhang, Q. Han, J. Liu, S. Zauscher, D. B. Mitzi, *Inorg. Chem.* **2017**, *56*, 9291.
[6] C. Katan, N. Mercier, J. Even, *Chem. Rev.* **2019**, *119*, 3140.
[7] M. Dyksik, H. Duim, X. Zhu, Z. Yang, M. Gen, Y. Kohama, S. Adjokatse, D. K. Maude, M. A. Loi, D. A. Egger, M. Baranowski, P. Plochocka, *ACS Energy Lett.* **2020**, *5*, 3609.
[8] H. H. Fang, J. Yang, S. Adjokatse, E. Tekelenburg, M. E. Kamminga, H. Duim, J. Ye, G. R. Blake, J. Even, M. A. Loi, *Adv. Funct. Mater.* **2020**, *30*, 1907979.
[9] T. T. H. Do, A. Granados del Águila, D. Zhang, J. Xing, S. Liu, M. A. Prosnikov, W. Gao, K. Chang, P. C. M. Christianen, Q. Xiong, *Nano Lett.* **2020**, *20*, 5141.
[10] S. Kahmann, E. K. Tekelenburg, H. Duim, M. E. Kamminga, M. A. Loi, *Nat. Commun.* **2020**, *11*, 2344.
[11] D. B. Straus, S. Hurtado Parra, N. Iotov, J. Gebhardt, A. M. Rappe, J. E. Subotnik, J. M. Kikkawa, C. R. Kagan, *J. Am. Chem. Soc.* **2016**, *138*, 13798.
[12] A. R. Srimath Kandada, D. Beljonne, C. Silva, A. Petrozza, F. Thouin, D. A. Valverde-Chávez, C. Quarti, D. Cortecchia, I. Bargigia, *Nat. Mater.* **2018**, *18*, 349.
[13] D. B. Straus, N. Iotov, M. R. Gau, Q. Zhao, P. J. Carroll, C. R. Kagan, *J. Phys. Chem. Lett.* **2019**, *10*, 1198.
[14] D. B. Straus, S. Hurtado Parra, N. Iotov, Q. Zhao, M. R. Gau, P. J. Carroll, J. M. Kikkawa, C. R. Kagan, *ACS Nano* **2020**, *14*, 3621.
[15] G. Folpini, D. Cortecchia, A. Petrozza, A. R. Srimath Kandada, *J. Mater. Chem. C* **2020**, *8*, 10889.
[16] E. K. Tekelenburg, S. Kahmann, M. E. Kamminga, G. R. Blake, M. A. Loi, *Adv. Opt. Mater.* **2021**, 2001647, https://doi.org/10.1002/adom.202001647.
[17] D. H. Fabini, R. Seshadri, M. G. Kanatzidis, *MRS Bull.* **2020**, *45*, 467.
[18] L. Zhang, X. Zhang, G. Lu, *J. Phys. Chem. Lett.* **2020**, *11*, 6982.
[19] M. G. Goesten, R. Hoffmann, *J. Am. Chem. Soc.* **2018**, *140*, 12996.
[20] E. S. Parrott, T. Green, R. L. Milot, M. B. Johnston, H. J. Snaith, L. M. Herz, *Adv. Funct. Mater.* **2018**, *28*, 1802803.
[21] S. Kahmann, S. Shao, M. A. Loi, *Adv. Funct. Mater.* **2019**, *29*, 1902963.
[22] J. M. Urban, G. Chehade, M. Dyksik, M. Menahem, A. Surrente, G. Trippé-Allard, D. K. Maude, D. Garrot, O. Yaffe, E. Deleporte, P. Plochocka, M. Baranowski, *J. Phys. Chem. Lett.* **2020**, *11*, 5830.
[23] R. G. Niemann, A. G. Kontos, D. Palles, E. I. Kamitsos, A. Kaltzoglou, F. Brivio, P. Falaras, P. J. Cameron, *J. Phys. Chem. C* **2016**, *120*, 2509.
[24] B. Dhanabalan, Y.-C. Leng, G. Biffi, M.-L. Lin, P.-H. Tan, I. Infante, L. Manna, M. P. Arciniegas, R. Krahne, *ACS Nano* **2020**, *14*, 4689.
[25] K. Uchinokura, T. Sekine, E. Matsuura, *J. Phys. Chem. Solids* **1974**, *35*, 171.
[26] L. Ni, U. Huynh, A. Cheminal, T. H. Thomas, R. Shivanna, T. F. Hinrichsen, S. Ahmad, A. Sadhanala, A. Rao, *ACS Nano* **2017**, *11*, 10834.
[27] A. Simbula, R. Pau, Q. Wang, F. Liu, V. Sarritzu, S. Lai, M. Lodde, F. Mattana, G. Mula, A. Geddo Lehmann, I. D. Spanopoulos, M. G. Kanatzidis, D. Marongiu, F. Quochi, M. Saba, A. Mura, G. Bongiovanni, *Adv. Opt. Mater.* **2021**, *2100295*, 2100295.
[28] Y. Kato, D. Ichii, K. Ohashi, H. Kunugita, K. Ema, K. Tanaka, T. Takahashi, T. Kondo, *Solid State Commun.* **2003**, *128*, 15.
[29] K. Tanaka, T. Takahashi, T. Kondo, K. Umeda, K. Ema, T. Umebayashi, K. Asai, K. Uchida, N. Miura, *Jpn. J. Appl. Phys.* **2005**, *44*, 5923.
[30] T. Goto, H. Makino, T. Yao, C. H. Chia, T. Makino, Y. Segawa, G. A. Mousdis, G. C. Papavassiliou, *Phys. Rev. B* **2006**, *73*, 115206.
[31] S. Neutzner, F. Thouin, D. Cortecchia, A. Petrozza, C. Silva, A. R. Srimath Kandada, *Phys. Rev. Mater.* **2018**, *2*, 064605.
[32] J. Li, J. Wang, J. Ma, H. Shen, L. Li, X. Duan, D. Li, *Nat. Commun.* **2019**, *10*, 806.
[33] M. Wang, J. Tang, H. Wang, C. Zhang, Y. S. Zhao, J. Yao, *Adv. Opt. Mater.* **2020**, *8*, 1901780.

[34] R. A. DeCrescent, X. Du, R. M. Kennard, N. R. Venkatesan, C. J. Dahlman, M. L. Chabinyc, J. A. Schuller, *ACS Nano* **2020**, *14*, 8958.
[35] R. A. DeCrescent, N. R. Venkatesan, C. J. Dahlman, R. M. Kennard, X. Zhang, W. Li, X. Du, M. L. Chabinyc, R. Zia, J. A. Schuller, *Sci. Adv.* **2020**, *6*, eaay4900.
[36] J. Li, J. Ma, X. Cheng, Z. Liu, Y. Chen, D. Li, *ACS Nano* **2020**, *14*, 2156.
[37] R. F. Moral, J. C. Germino, L. G. Bonato, D. B. Almeida, E. M. Therézio, T. D. Z. Atvars, S. D. Stranks, R. A. Nome, A. F. Nogueira, *Adv. Opt. Mater.* **2020**, *8*, 2001431.
[38] A. Francisco-López, B. Charles, M. I. Alonso, M. Garriga, M. T. Weller, A. R. Goñi, *Adv. Opt. Mater.* **2021**, 2001969, https://doi.org/10.1002/adom.202001969.
[39] M. Seitz, M. Meléndez, N. Alcázar-Cano, D. N. Congreve, R. Delgado-Buscalioni, F. Prins, *Adv. Opt. Mater.* **2021**, *2001875*, 2001875.
[40] D. W. DeQuilettes, W. Zhang, V. M. Burlakov, D. J. Graham, T. Leijtens, A. Osherov, V. Bulović, H. J. Snaith, D. S. Ginger, S. D. Stranks, *Nat. Commun.* **2016**, *7*, 11683.
[41] E. Mosconi, D. Meggiolaro, H. J. Snaith, S. D. Stranks, F. De Angelis, *Energy Environ. Sci.* **2016**, *9*, 3180.
[42] M. Liu, O. Voznyy, R. Sabatini, F. P. García de Arquer, R. Munir, A. H. Balawi, X. Lan, F. Fan, G. Walters, A. R. Kirmani, S. Hoogland, F. Laquai, A. Amassian, E. H. Sargent, *Nat. Mater.* **2016**, *16*, 258.
[43] F. Jiang, J. Pothoof, F. Muckel, R. Giridharagopal, J. Wang, D. S. Ginger, *ACS Energy Lett.* **2021**, *6*, 100.
[44] N. Miura, K. Uchida, T. Yasuhira, E. Kurtz, C. Klingshirn, H. Nakashima, F. Issiki, Y. Shiraki, *Phys. E Low-Dimens. Syst. Nanostruct.* **2002**, *13*, 263.
[45] T. Neumann, S. Feldmann, P. Moser, J. Zerhoch, T. van de Goor, A. Delhomme, T. Winkler, J. J. Finley, C. Faugeras, M. S. Brandt, A. V. Stier, F. Deschler, *arXiv:2009.13867* **2020**.
[46] N. Miura, *Physics of Semiconductors in High Magnetic Fields*, Oxford University Press, Oxford **2007**.
[47] C. Zhang, D. Sun, C.-X. Sheng, Y. X. Zhai, K. Mielczarek, A. Zakhidov, Z. V. Vardeny, *Nat. Phys.* **2015**, *11*, 427.